Electronic Supplementary Information (ESI) for "Homogeneous nucleation of carbon dioxide in supersonic nozzles II: molecular dynamics simulations and properties of nucleating clusters" by Halonen et al.

List of ESI figures

Nucleation rate and threshold value

The nucleation rates are determined from the simulation data using the Yasuoka-Matsumoto method, in which the appearance of clusters above some threshold size, $\bar{n}$, is monitored in time. Ideally the chosen threshold size should not affect the obtained value of the nucleation rate if it is larger than the critical size, but this is not completely true as the simulated vapour is very dense and a substantial fraction of the monomers is depleted during the simulations. As illustrated in Fig. S1, the nucleation rate, *i.e.* the slope of the curve, decreases slightly with increasing threshold size.

In addition, to determine the time over which nucleation takes place, we have arbitrarily defined the nucleation stage as the period when the number of clusters over the threshold size lies between 20 % and 80 % of the maximum value reached in the simulation. The nucleation stage for $\bar{n} = 5$ is indicated by the shaded gray areas in Fig. S1.

As the slopes in Fig. S1 decrease monotonically as $\bar{n}$ increases, we have tried to find the most similar slopes for our analysis. First, we reject the smallest threshold sizes until the difference between the slopes of two consecutive threshold sizes is below 10 %. The next four smallest threshold sizes are then used to calculate the average nucleation rate J presented in Table 2. The smallest threshold sizes are 7, 9 and 11 at temperatures 75, 90 and 105 K, respectively. Even though this method is quite simple, the standard deviation in J is only about 10 %.

Kinetic energy distributions and cluster excess energy q_n

By using the principles of energy and momentum conservation, we can express the excess energy of a nucleating n-cluster after a collision between a monomer and $(n-1)$-cluster as:

$$q_n = U_{n-1} - U_n, \tag{S1}$$

where U_n is the potential energy at the bath temperature (*i.e.* with harmonic correction). Any possible anharmonicities are cancelled out due to recursion, this can be demonstrated by comparing eqn (S1) with an analogous expression for the total energies:

$$q = E_{n-1} - E_n + \frac{5}{2}RT, \tag{S2}$$

where an additional term, $5/2RT$, is introduced to account for the vibrational energy. We found that the difference between q_n values calculated using either eqn (S1) or eqn (S2) is less than 1 %.

For simplicity, the size-dependency of q_n can be parameterised using the liquid-drop model ($U_n = An + Bn^{2/3}$):

$$q_n = -A - B(n^{2/3} - (n-1)^{2/3}), \tag{S3}$$

where the coefficients A and B are the vertical intercept and the slope of the U/n-curve shown in Fig. 6, S5 and S6. The average coefficients (A,B) at 75, 90 and 105 K are $(-4.64, 5.82)$, $(-4.44, 5.67)$ and $(-4.21, 5.55)$, respectively (in units of kcal/mol). The obtained q_n-values (from eqn (S1) and (S3)) for each simulation systems are shown in Fig. S4.

Lindemann index analysis

One measure of phase state of the clusters is the Lindemann index, which is used to distinguish different phases based on the atomic mobility. For a system of n atoms, the Lindemann index, Δ, is defined as [1]

$$\Delta = \frac{1}{n(n-1)} \sum_{j \neq i}^{n} \frac{\sqrt{\langle r_{i,j}^2 \rangle - \langle r_{i,j} \rangle^2}}{\langle r_{i,j} \rangle}, \tag{S4}$$

where $r_{i,j}$ is the distance between atoms i and j, and $\langle \ldots \rangle$ denotes a time average. Typically, a threshold value $\Delta \approx 0.1 \ldots 0.2$ is used to separate liquid and solid phases.

Here we have calculated the Lindemann index only for carbon atoms. Lindemann indices calculated for nucleating (NVE simulated) and equilibrated (NVT) clusters at $T = 75$ K are shown in Fig. S7. The large nucleating clusters ($n > 10$) reach a steady value of $\Delta \approx 0.33$, while the smaller nucleating clusters exhibit slightly smaller values of Δ. Frantz [2,3] has reported very similar values for liquid Lennard-Jones clusters at the proximity of the phase transition region. According to Frantz [3], a threshold value $\Delta = 0.2$ is most suitable for small clusters.

Based on Fig. S7, the calculated values of Δ for the very stable equilibrium clusters ($n = 13$, 25, 28 and $n > 32$) are well below the threshold value, indicating clear solid-like behaviour. This is expected, as the reported melting temperature of 13-clusters is about 95 K [4]. The Δ values of the intermediate cluster sizes ($n = 14 \ldots 24$ and $30 \ldots 32$) are close to the threshold value of 0.2, but the thermal motion is significantly decreased compared to the corresponding nucleating clusters. No such clear difference in thermal motion can be seen for pre-icosahedral clusters ($n < 13$) as Δ is very similar for both NVE and NVT simulated clusters. The corresponding Monte Carlo simulations of Frantz [2], demonstrate a clear phase transition from solid to liquid even for the smallest clusters (e.g. in case of a 6-cluster, the value of Δ jumps from ~ 0.01 to over 0.2 after the phase transition). Thus, based on both results shown in Fig. S7 and earlier results by Frantz [2], it is evident that the smallest CO_2 clusters are liquid-like at $T = 75$ K or higher.

Thermophysical properties used in the study

Table S1 Thermophysical properties of CO_2, the TraPPE model of CO_2 and argon

Molecule	Property	Unit	Value	Ref.
CO_2	m	g/mol	44	
	P^{eq}	Pa	$101325 \times 10^{-1353.202/T-8.142537 \log T+6.259156\times10^{-3}T+24.6193}$	5
	ρ_{l}	kg/m^3	$467.6\prod_{i=1}^{4}\exp(a_i(1-T/304.1282)^{t_i})$; $a_1 = 1.9245108$, $a_2 = -0.62385555$, $a_3 = -0.32731127$, $a_4 = 0.39245142$, $t_1 = 0.34$, $t_2 = 0.5$, $t_3 = 10/6$ and $t_4 = 11/6$	6
	σ_{Quinn}	mN/m	$0.0653(304.5-T)^{1.24}$	7
	σ_{LH}	mN/m	$0.23425T(304.2/T-1)^{1.21}$	8,9
CO_2 (TraPPE)	m	g/mol	44	
	P^{eq}	Pa	$\exp(22.538-2024.756T^{-1})$	10
Ar	m_{Ar}	g/mol	40	

Notes and references

1 K. Hansen, *Statistical physics of nanoparticles in the gas phase*, Springer International Publishing, 2nd edn., 2018.

2 D. D. Frantz, *J. Chem. Phys.*, 1995, **102**, 3747–3768.

3 D. D. Frantz, *J. Chem. Phys.*, 2001, **115**, 6136–6157.

4 J.-B. Maillet, A. Boutin, S. Buttefey, F. Calvo and A. H. Fuchs, *J. Chem. Phys.*, 1998, **109**, 329–337.

5 A. Michels, T. Wassenaar, T. Zwietering and P. Smits, *Physica*, 1950, **16**, 501–504.

6 R. Span and W. Wagner, *J. Phys. Chem. Ref. Data*, 1996, **25**, 1509–1596.

7 E. L. Quinn, *J. Am. Chem. Soc.*, 1927, **49**, 2704–2711.

8 J. Lielmezs and T. Herrick, *Chem. Eng. J.*, 1986, **32**, 165–169.

9 K. K. Dingilian, R. Halonen, V. Tikkanen, B. Reischl, H. Vehkamäki and B. E. Wyslouzil, *Phys. Chem. Chem. Phys.*, 2020, **22**, 19282–19298.

10 J. J. Potoff and J. I. Siepmann, *AIChE J.*, 2001, **47**, 1676–1682.

11 H. Takeuchi, *J. Phys. Chem. A*, 2008, **112**, 7492–7497.

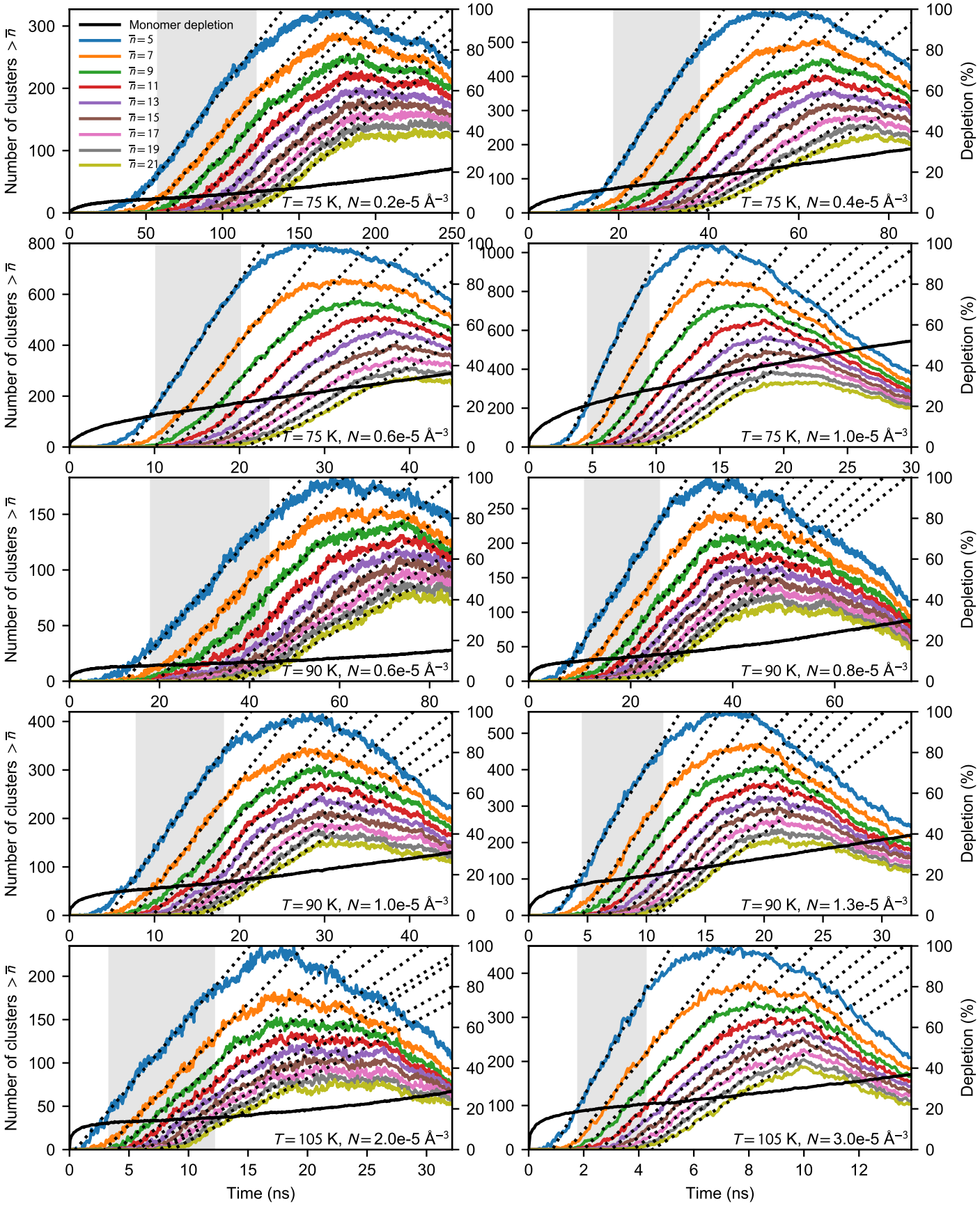

Fig. S1 Time-evolution of the total number of clusters larger than the threshold size $\bar{n}$ for different combinations of temperature and density (colored lines). The linear fits, whose slopes correspond to τ, are shown as dotted lines. The black solid line shows the level of monomer depletion D during the simulation. The "nucleation stage" for $\bar{n}=5$, *i.e.*, the time period over which the average monomer density was calculated, is indicated by the shaded gray area.

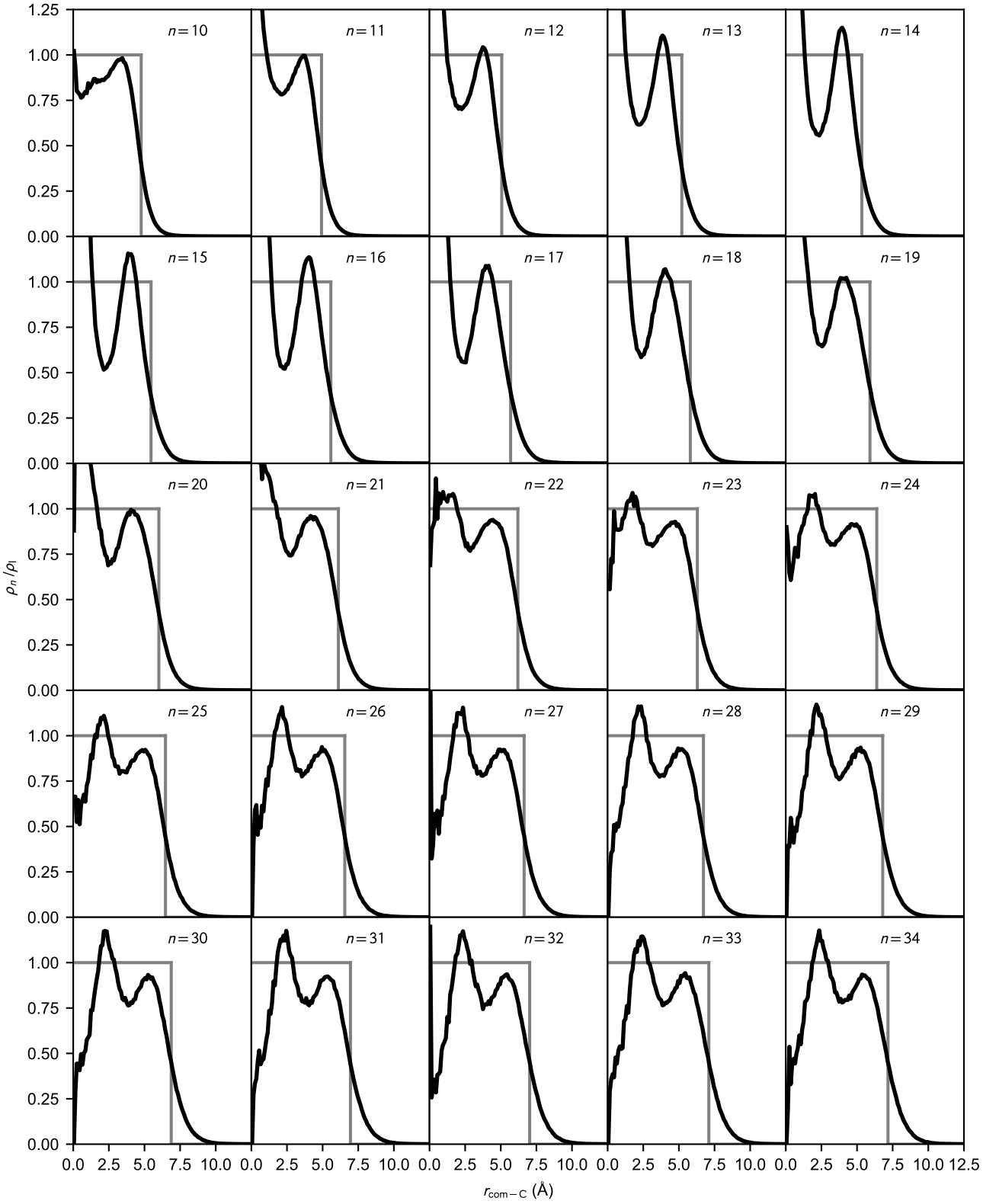

Fig. S2 Normalized radial carbon atom density inside nucleating clusters at 75 K as a function of the distance from the cluster's centre of mass (black lines), for cluster sizes $n = 10 \ldots 34$. The gray line illustrates the density profile estimated using the liquid-drop model and bulk liquid density ρ_l.

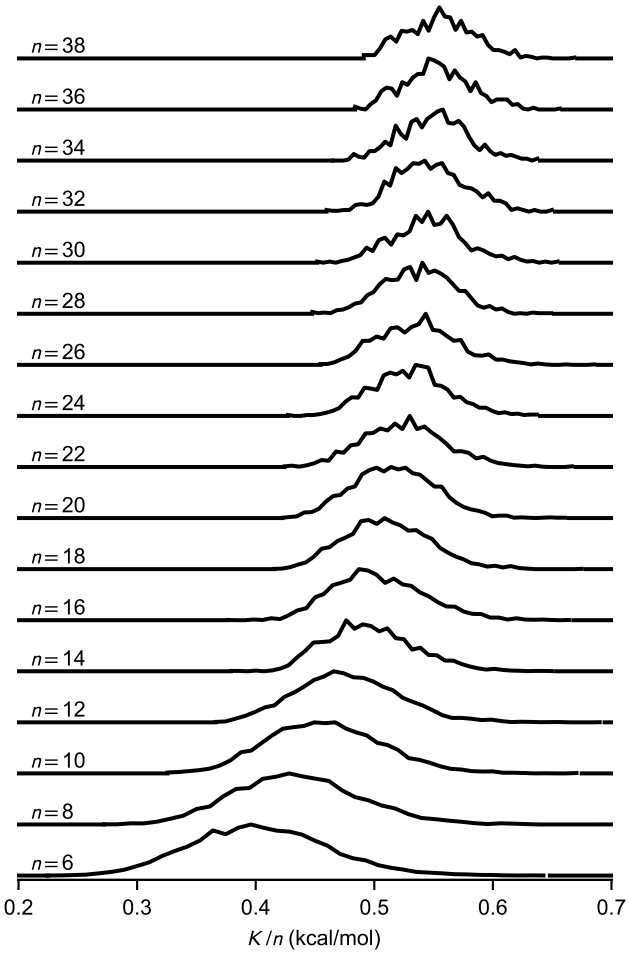

Fig. S3 Distributions of kinetic energy per molecule for cluster sizes $n = 6 \ldots 38$, at $T = 75$ K and $N = 0.2 \times 10^{-5}$ Å^{-3}.

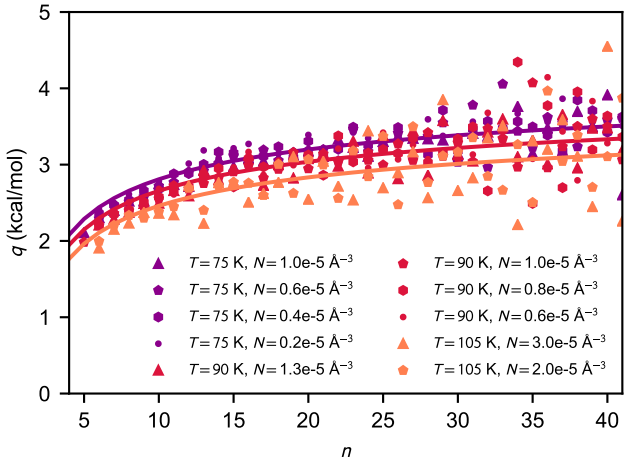

Fig. S4 Excess energy q as a function of cluster size n calculated from the cluster potential energies obtained from the nucleation simulations. The solid lines correspond to eqn (S3) at the respective temperature.

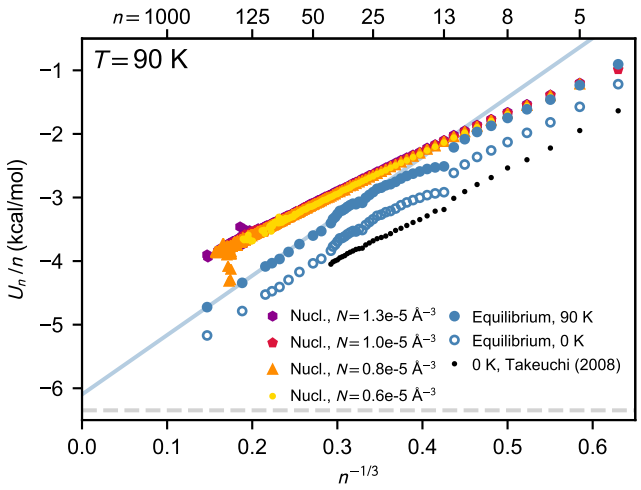

Fig. S5 Potential energy per molecule as a function of $n^{-1/3}$ for clusters isolated from nucleation simulations carried out at 90 K. The energies of the nucleating clusters at different vapour densities (from NVE simulations, harmonically scaled to 90 K) are shown as coloured dots, triangles, pentagons and hexagons, and the equilibrated cluster energies (from NVT simulations) are indicated as filled blue circles. The blue solid line shows the extrapolated $n^{-1/3}$ dependence for the large equilibrated clusters. The bulk FCC cohesive energy value at 90 K is shown by the horizontal dashed line. The open circles illustrate the equilibrated potential energies harmonically scaled to 0 K, and the black dots are the geometry optimized global minimum energies obtained by Takeuchi [11].

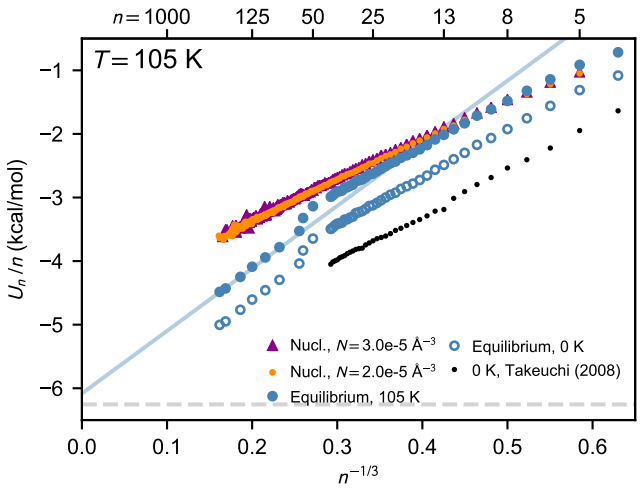

Fig. S6 Potential energy per molecule as a function of $n^{-1/3}$ for clusters isolated from nucleation simulations carried out at 105 K. The symbols and colours are the same as in Fig. S5.

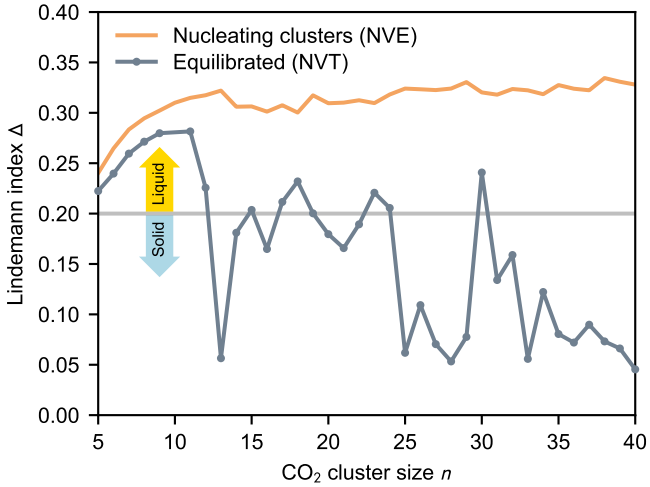

Fig. S7 Calculated Lindemann indices for nucleating (NVE simulated) and equilibrated clusters (NVT) at $T = 75$ K. The threshold value of 0.2 suggested by Frantz [3] is indicated by the gray horizontal line.

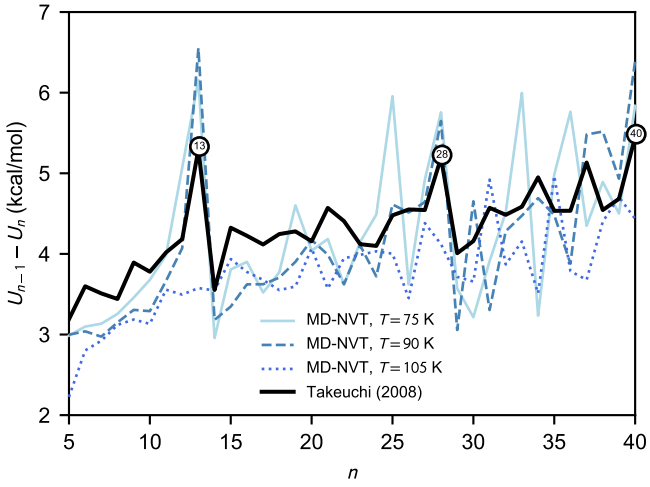

Fig. S8 Potential energy difference of two adjacent cluster sizes for CO_2 clusters equilibrated at 75, 90 and 105 K (blue lines). The global minimum values by Takeuchi [11] are shown as thick black line. The stable cluster sizes ($n = 13$, 28 and 40) are labeled in black circles.